

PAPER • OPEN ACCESS

## Influence of thermophysical properties of working fluid on the design of cryogenic turboexpanders using $n_s d_s$ diagram

To cite this article: Ashish A Sam and Parthasarathi Ghosh 2015 *IOP Conf. Ser.: Mater. Sci. Eng.* **101** 012179

View the [article online](#) for updates and enhancements.

### Related content

- [Models of thermophysical properties of uranium dioxide](#)  
Yu N Devyatko, V V Novikov, V I Kuznetsov et al.
- [Characterization of structure and thermophysical properties of three ESR slags](#)  
A. Plotkowski, J. deBarbadillo and Matthew J. M. Krane
- [Thermophysical properties of ethylene glycol mixture based CNT nanofluids](#)  
D M Camarano, F A Mansur, T L C F Araújo et al.

### Recent citations

- [Effect of rotation on the flow behaviour in a high-speed cryogenic microturbine used in helium applications](#)  
Ashish Alex Sam *et al*
- [Flow field analysis of high-speed helium turboexpander for cryogenic refrigeration and liquefaction cycles](#)  
Ashish Alex Sam and Parthasarathi Ghosh
- [Effect of trailing edge thickness on the performance of a helium turboexpander used in cryogenic refrigeration and liquefaction cycles](#)  
Ashish Alex Sam and Parthasarathi Ghosh



**ECS** **240th ECS Meeting**  
Oct 10-14, 2021, Orlando, Florida

**Register early and save up to 20% on registration costs**

Early registration deadline Sep 13

**REGISTER NOW**

# Influence of thermophysical properties of working fluid on the design of cryogenic turboexpanders using $n_s d_s$ diagram

Ashish A Sam, Parthasarathi Ghosh\*

Cryogenic Engineering Centre, Indian Institute of Technology Kharagpur, India - 721302

E-mail: s.partha.ghosh@gmail.com

**Abstract.** Cryogenic turboexpanders are an essential part of liquefaction and refrigeration plants. The thermodynamic efficiency of these plants depends upon the efficiency of the turboexpander, which is the main cold generating component of these plants, and therefore, they should be designed for high thermodynamic efficiencies. Balje's [1]  $n_s d_s$  chart, which is a contour of isentropic efficiencies plotted against specific speed and specific diameter, is commonly used for the preliminary design of cryogenic turboexpanders. But, these charts were developed based on calculations for a specific heat ratio ( $\gamma$ ) of 1.4, and studies show that care should be taken while implementing the same for gases which have a higher  $\gamma$  of 1.67. Hence there is a need to investigate the extent of applicability of  $n_s d_s$  diagram in designing expansion turbines for higher specific heat ratios. In this paper, Computational Fluid Dynamics (CFD) analysis of cryogenic turboexpanders was carried out using Ansys CFX<sup>®</sup>. The turboexpanders were designed based on the methodologies prescribed by Kun and Sentz [2] following the  $n_s d_s$  diagram of Balje and Hasselgruber's technique for generating blade profile. The computational results of the two cases were analysed to investigate the applicability of Balje's  $n_s d_s$  diagram for the design of turboexpanders for refrigeration and liquefaction cycles.

## 1. Introduction

The low volumetric flow rate and variation of thermophysical properties at low temperatures makes the design of a cryogenic turboexpander for liquefaction systems demanding. Lower volumetric flow rate means a smaller turbine size and higher turbine wheel speed which in turn makes the flow more complex [3]. The most commonly used conventional turbomachinery blade design methods include 1D preliminary design, 1D meanline analysis followed by 2D inverse blade design procedures [4]. With the advent of CFD and high performance computing capabilities, the use of 3D viscous flow analysis for turbomachinery design has also now become quite common [5,6].

The preliminary design is the very first step in the design procedure of turbomachines. The 1D preliminary design involves the use of similarity parameters, which in the form of performance charts, empirical data etc. can be used to describe the complete characteristics of the machine. The basic idea of using these similarity parameters is to use the optimised results of one unit for the design of other. The preliminary design methods provide calculations at the basic turbomachinery stations, focusing on the essential aspects of the flow without any intense computational procedure. It provides the basic flow path along the meridional streamline in addition to the performance prediction. As the assumptions made in the preliminary methods are input to the subsequent calculations, this method is



of prime importance, and any slight modifications can yield considerable improvement in the efficiency [3,7].

### 1.1 Balje's $n_s$ - $d_s$ chart

As stated earlier, the  $n_s$ - $d_s$  chart, as shown in figure 1, is a widely accepted approach for the prediction of turbomachinery efficiency and for the selection of design parameters [1]. A major advantage of Balje's representation is that the efficiency is shown as a function of parameters which are of immediate concern to the designer like angular speed and rotor diameter. It is a two dimensional vector diagram plotting isoefficiency contours against specific speed and specific diameter. Similarity principles that make use of performance charts like  $n_s$ - $d_s$  diagrams stipulate that machines that have the same specific speed, same specific diameter and similar design geometry will be dynamically equivalent and thus have the same efficiency, if Reynolds number and Mach number effects are neglected. This can be expressed as;

$$\eta = f(n_s, d_s, \text{geometrical parameters, } Re^*, La^*, \gamma)$$

Ghosh [3] has mentioned that the following observations should be taken into consideration while using Balje's  $n_s$ - $d_s$  diagram for the design of turbomachines: (1) The assumed efficiency value from Balje's chart is valid only when the Reynolds number is greater than  $2 \times 10^6$  and the Laval number is less than 1. For values outside this range, efficiency de-rating factors should be used. (2) Efficiency penalties should also be introduced in case of stress-limited wheels, wet turboexpanders and sub-optimum installations. (3) As the Balje's chart was developed based on certain values of clearance ratio, trailing edge ratio and surface roughness ratio, the maximum efficiency can be achieved only when these geometrical similarities are conserved. (4) The accuracy of the loss correlations is important as it influences the exactness of the computed efficiency. (5) Macchi [7] has shown that as the Balje's  $n_s$ - $d_s$  diagram was obtained for a working fluid with a  $\gamma = 1.41$ , the chart needs to be modified for it to be used for working fluids with higher  $\gamma$ .

For cryogenic turboexpanders a design methodology based on Balje's  $n_s$ - $d_s$  diagram [1] has been developed [3,8] and suggested by Kun and Sentz [2]. For the current effort the blade shape is generated by a methodology prescribed by Hasselgruber [9]. The design procedure has been used for turbines with nitrogen and helium as the working fluid.

### 1.2 Objective

As shown by Macchi [7], for working fluids with  $\gamma$  other than 1.41, Balje's chart needs to be modified. Hence, there is a need to verify the applicability of Balje's  $n_s$ - $d_s$  chart for the design of turboexpanders with the working fluid having a higher  $\gamma$ . The objective of this paper is to compare the performance of cryogenic turboexpanders designed for two different working fluids, one with nitrogen and the other with helium, through CFD analysis. The performance and design parameters obtained through CFD analysis are compared with 1D design values to bring out the differences in these parameters for the two turbines. Thus the extent of applicability of the  $n_s$ - $d_s$  diagram for designing a helium turboexpander can be realized.

## 2. Methodology

### 2.1 Design of cryogenic turboexpander

The cryogenic turboexpander in refrigeration and liquefaction cycles constitute an inlet nozzle for guiding the flow, a  $90^\circ$  inward flow radial turbine and a diffuser for recovering the pressure. In the present cases the preliminary design of the turboexpanders was made based on Balje's  $n_s$ - $d_s$  chart and one dimensional meanline analysis was done following Kun and Sentz' [2] design methodology. The turbine wheel blade profile was generated following Hasselgruber's technique [9] and that proposed by Balje [1]. The 3D model of the turboexpander is shown in figure 2.

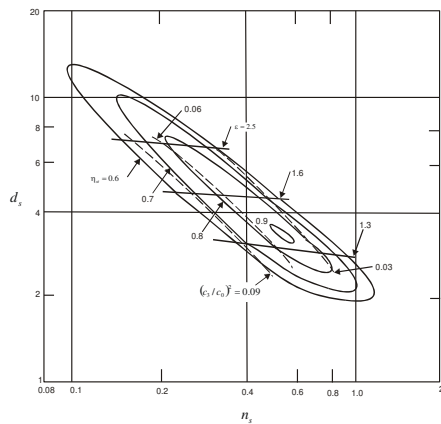


**Figure 1.** Balje's  $n_s$ - $d_s$  chart [1]

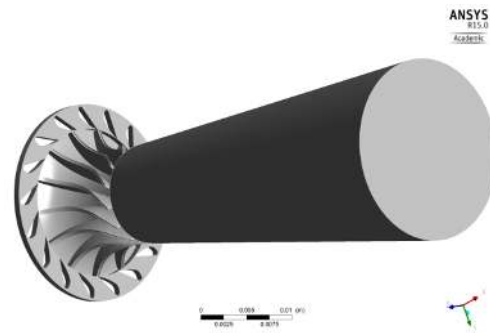


**Figure 2.** 3D model of cryogenic turboexpander

## 2.2 Geometry and grid

The 3D model of the turbine wheel was developed using ANSYS BladeGen<sup>®</sup> and was meshed using ANSYS TurboGrid<sup>®</sup>. A structured mesh with a combination of hexahedral and tetrahedral elements was used for meshing the turbine wheel. The inlet nozzle and the diffuser section were modelled using ANSYS DesignModeler<sup>®</sup> and ANSYS CFX-Mesh<sup>®</sup> was employed to generate the mesh. The features of the mesh along with the total number of elements and nodes in each component of the turboexpander are mentioned in table 1. This was done based on a grid independence test to study the influence of grid size on the results. For this three different meshes were used and their results were compared. Considering the computational time and the negligible difference in the results of the meshes between type B and C, type B mesh was therefore used in the current study. To ensure sufficient grid refinement at the boundary, the  $y^+$  value was kept around 1 at all the boundaries. The grid independence study for helium turboexpander is shown in table 2.

**Table 1.** Mesh specifications for various components

	Domain	Number of nodes	Method	Mesh type/ type of elements
Nitrogen	Nozzle	101728	Sweep	Unstructured/ Hexahedral, small no. of wedges
	Turbine	1920192	ATM optimized	Structured (H and O type topology)/ Hexahedral only
	Diffuser	585570	Patch conforming method	Unstructured/ Tetrahedral
Helium	Nozzle	769033	Sweep	Unstructured/ Hexahedral, small no. of wedges
	Turbine	3449979	ATM optimized	Structured (H and O type topology)/ Hexahedral only
	Diffuser	769287	Patch conforming method	Unstructured/ Tetrahedral

**Table 2.** Grid independent test for helium turboexpander

Grid type	Total number of nodes (in millions)	Turbine efficiency (total to static)	Computational time
A	1.94	68.98	6 hours 13 minutes
B	5.01	72.28	12 hours 3 minutes
C	14.80	72.73	15 hours 49 minutes

### 2.3 Boundary conditions

The boundary conditions for the CFD analysis of the turboexpanders are given in table 3. The nozzle inlet was considered as the inlet boundary and the exit of the diffuser as the outlet boundary. The mass flow rate and inlet total temperature were specified at the inlet whereas the static pressure was specified at the outlet.

**Table 3.** Turboexpander specification

	Nitrogen turboexpander	Helium turboexpander
Total pressure at inlet	6 bar	16.5 bar
Total temperature at inlet	120 K	70 K
Mass flow rate	0.06 kg/s	0.05 kg/s
Static pressure at exit	1.5 bar	11 bar
Rotational speed	120000 rpm	264000 rpm
Specific speed	0.548	0.587
Specific diameter	3.54	3.14
Machine Reynolds number	$7.75 \times 10^6 > 2 \times 10^6$	$4.48 \times 10^6 > 2 \times 10^6$
Laval number	$0.96 < 1$	$0.52 < 1$

### 2.4 Numerical model

The CFD solver ANSYS-CFX<sup>®</sup> was used for the steady state viscous flow simulations, where the RANS (Reynolds–Averaged Navier–Stokes) equation based SST (Shear Stress Transport) turbulence model with automatic wall treatment was used for turbulence closure. This model showed good agreement with the experimental results where similar kinds of turbomachines were used [10, 11]. The validation of the computational approach used in this paper is presented in an earlier work, currently under review [12]. The automatic wall treatment function will automatically switch between the low Reynolds number boundary layer formulation and the wall function, based on the grid refinement at the boundary. The SST model is a combination of the best elements of the  $k$ - $\epsilon$  and  $k$ - $\omega$  model [13] and therefore accurately predicts the boundary layer flow and separation. It takes into account the transport of the principal turbulent shear stress and therefore accurately predicts the adverse pressure gradients [14]. The Peng-Robinson cubic equation of state was used to describe the properties of nitrogen, and for helium the ideal gas equation of state was employed [15]. In the present simulation the turbulent intensity was assumed to be 5%, and all the walls were assumed to be smooth, adiabatic and having no slip.

### 2.5 Rotor stator interface

The interface between the stationary (nozzle and diffuser) and rotating (turbine wheel) parts requires special treatment due to the rotor – stator interactions in turbomachines. As the turbomachinery flow is highly turbulent and unsteady, transient simulations are required to completely capture the flow physics. But this requires enormous computational effort and the use of high performance computers. This has resulted in different steady state simulation approaches. In our present case the frozen rotor model was used to model the rotor stator interface where the rotor-stator position remains fixed throughout the simulation. Although the model partly accounts for the interactions, the transient effects still remain unresolved [16]. The simulations were carried out until the residuals decreased to  $10^{-4}$  (Root Mean Square) for all the conservation equations. The convergence of the solutions was ensured by monitoring the residual values and variables of interest.

## 3. Results and Discussion

The turboexpanders in the present case maintain geometric similarity and the Machine Reynolds number and the Laval number were within the valid range as suggested by Balje (table 3). The only other parameter that influences the efficiency according to the equations is  $\gamma$  of the fluids. The value of  $\gamma$  is different for the two fluids. Therefore any differences in the performance and flow characteristics

in the two cases may be attributed to this difference in  $\gamma$  values. The CFD analyses for the cryogenic turboexpanders were performed and the performance and design parameters obtained were compared with 1D design values for both the expanders (table 4). This table shows that the nozzle efficiency from CFD analysis for both cases is comparable, whereas in the case of the turbine wheel, the helium turbine efficiency through CFD analysis is higher. To analyse the impact of diffuser performance on the turboexpander efficiency, the total to static efficiency was also calculated excluding the diffuser i.e., at the rotor exit. The diffuser pressure recovery factor values reveals that the diffuser performance in the case of nitrogen is poor as compared to that of the helium turboexpander. However, the performance analysis in table 4 is not fully sufficient to discern the applicability of Balje's  $n_s$ - $d_s$  chart for the helium turboexpander design. This requires a thorough understanding of the various sources of efficiency degradation in the turboexpanders. For this, the entropy contours and velocity vectors in the blade to blade and stream wise locations were plotted for both the turboexpanders.

### 3.1 Tip clearance loss

The velocity vector plots in figure 3, which is near the trailing edge, exhibits the presence of vortex flows in the turboexpanders. A better comprehension of these vortex flows can be gained through the stream wise entropy contours shown in figures 4 and 5. The static entropy contours were plotted at three different stream wise locations from the leading to the trailing edge. It can be seen that the vortex originates at the suction side near the shroud tip and as the flow propagates it gets strengthened and shifts towards the mid passage. A closer look at these entropy contours reveals that the entropy generated due to the vortex flow in the helium turboexpander is higher than that in nitrogen turboexpander. Figure 6, which shows the velocity vectors in the blade to blade view nearer to the shroud tip, shows the strong cross flow from the pressure side to the suction side of the blade through the tip clearance which in turn results in the formation of vortex nearer the leading edge. Ghosh [1] has pointed out that the fluid flow through the shroud clearance will affect the turboexpanders performance due to leakage from the pressure side to the suction side and frictional drag of shroud on

**Table 4.** Comparison of performance parameters of turboexpanders through CFD analysis with 1D design

Factor	Nitrogen turboexpander		Helium turboexpander	
	1D design value	CFD	1D design value	CFD
Nozzle efficiency	93%	97.05%	93%	96.46%
Turbine efficiency (total to static)	75% (from Balje's chart)	77.21%	65% (from Balje's chart)	72.28%
Turbine wheel efficiency (total to static) at turbine wheel exit	75% (from Balje's chart)	75.49%	65% (from Balje's chart)	67.31%
Power developed	1.73 kW	1.99 kW	1.8 kW	2.21 kW
Diffuser pressure recovery factor	0.7	0.37	0.7	0.73

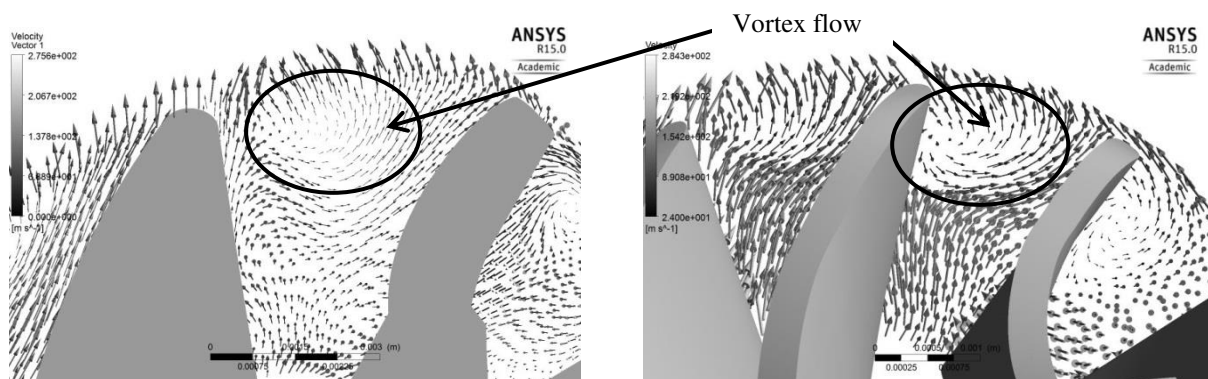


**Figure 3.** Velocity vectors near the trailing edge in the stream wise view (left) nitrogen turboexpander (right) helium turboexpander

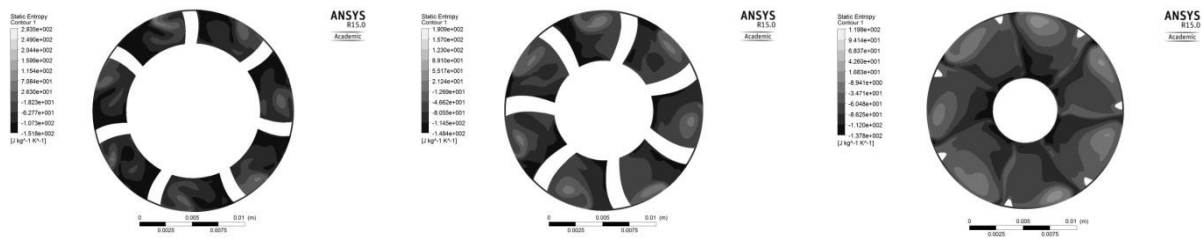


**Figure 4.** Entropy contour at different streamwise locations for nitrogen turboexpander

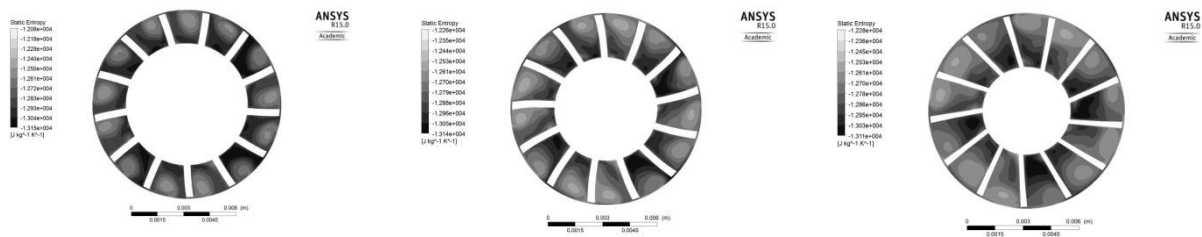


**Figure 5.** Entropy contour at different streamwise locations for helium turboexpander

the turbine wheel. The tip clearance for both the turboexpanders was set at 2% of the exit radius of the rotor (table 5). From the entropy contours in figure 7, it can be seen that the entropy generation due to tip leakage flow is greater in the helium turboexpander. This may be the result of greater tip leakage flow due to the lower viscosity of helium as compared to nitrogen. Minimization of the pressure gradient across the blade and tip leakage flow through the shroud tip clearance is possible through a modification of the blade profile and a reduction of the tip clearance height. Tip clearance height can either be kept constant or varied from the leading to the trailing edge, provided the stress and manufacturing constraints are taken into consideration. These geometrical modifications reduce the entropy generation due to tip leakage improving the turboexpander efficiency.

### 3.2 Trailing edge loss

This is another major source of loss in turboexpanders. Figure 8 depicts the entropy generated by the trailing edge vortices. Baines [17] has shown that the sudden expansion at the rotor exit results in flow separation and formation of vortices, which leads to the trailing edge loss. The entropy contour reveals that the entropy generation due to trailing edge vortices is greater in the helium turboexpander as compared to the nitrogen turboexpander. The geometric parameters of the turboexpanders used in this

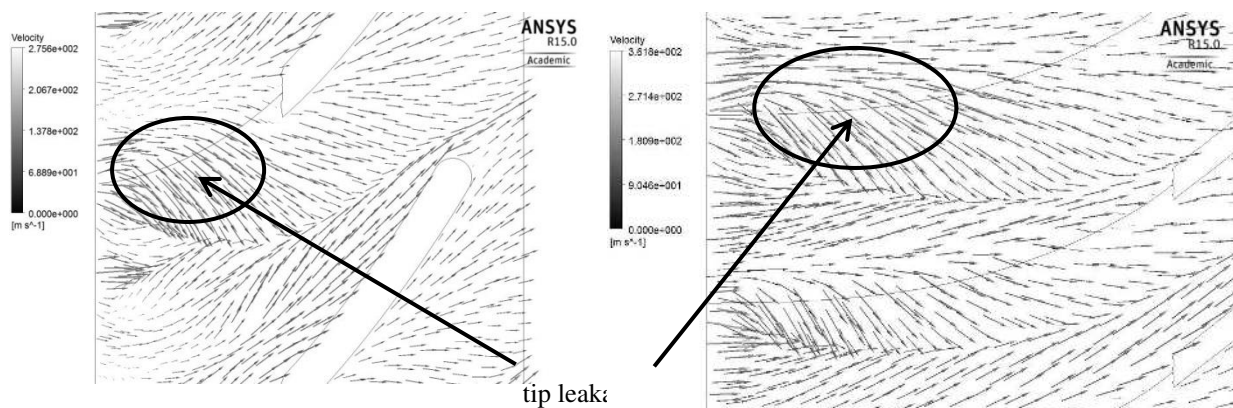


**Figure 6.** Velocity vector nearer to the shroud in the blade to blade view (left) nitrogen turboexpander (right) helium turboexpander

work are given in table 5. An optimised blade profile through quantification of entropy generation and detailed parametric analysis will help in minimizing the losses.

**Table 5.** Major geometrical parameters of the turboexpander

Parameter	Nitrogen turboexpander	Helium turboexpander
Impeller major diameter	26.232 mm	16 mm
Impeller tip diameter	18.092 mm	10.5 mm
Impeller hub diameter	6.332 mm	4.7 mm
Tip clearance	0.2 mm	0.1 mm

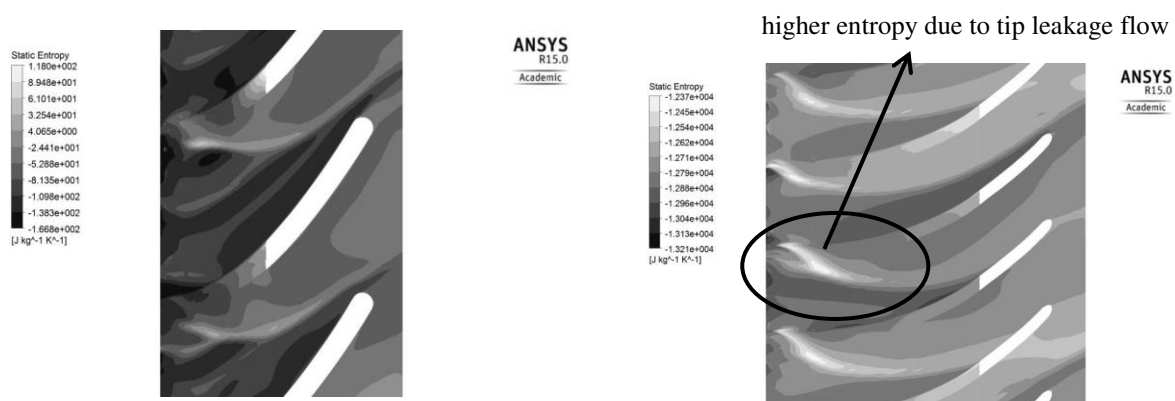


**Figure 7.** Entropy contour nearer to the shroud in the blade to blade view (left) nitrogen turboexpander (right) helium turboexpander

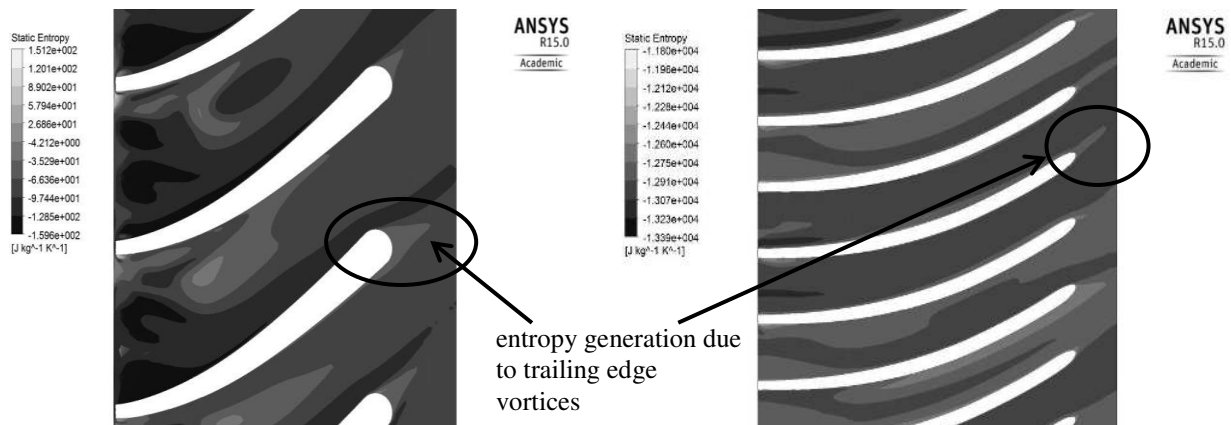


**Figure 8.** Entropy contour in the blade to blade view nearer to the hub (left) nitrogen turboexpander (right) helium turboexpander

#### 4. Conclusion

The CFD analyses of nitrogen and helium turboexpanders were performed, and the results were compared with 1D design values. The present study showed that there is considerable difference in the flow fields between nitrogen and helium turboexpanders that are designed based on  $n_s d_s$  diagram and Hasselgruber's method and the entropy generation in the helium turboexpander was greater as compared to that in the nitrogen turboexpander. This may be mainly due to the difference in the value of  $\gamma$ , as all the other design parameters were within the prescribed limit for the application of  $n_s d_s$  diagram. Therefore, the 1D preliminary design methodology for helium turboexpander needs to be

modified by incorporating the effect of thermophysical properties like viscosity and geometrical parameters like clearance ratio, and trailing edge ratio. The effect of  $\gamma$  on these differences will be further explored in the future. As the turbomachinery flow is highly turbulent and unsteady, transient analysis is required to completely capture the flow physics.

## Nomenclature

$C_p$  – diffuser pressure recovery factor

$$C_p = (P_{ex} - P_3)/(P_{0,3} - P_3)$$

$d_s$  – specific diameter

$$d_s = (D(h_{0,1} - h_{3,s})^{1/4})/\sqrt{Q_3}$$

$La^*$  – Laval number

$$La^* = U_2/\sqrt{(2\gamma RT_{0,1})/((\gamma + 1)M)}$$

$n_s$  – specific speed

$$n_s = (\omega\sqrt{Q_3})/(h_{0,1} - h_{3,s})^{3/4}$$

$P$  – power output of the turbine

$$P = \dot{m}(h_{0,1} - h_{0,ex})$$

$Re^*$  – machine Reynolds number

$$Re^* = U_2 D \rho_2 / \mu_2$$

$\eta_n$  – nozzle efficiency

$$\eta_n = (h_{0,1} - h_2)/(h_{0,1} - h_{2,s})$$

$\eta_{T-st}$  – total-to-static efficiency

$$\eta_{T-st} = (h_{0,1} - h_{0,ex})/(h_{0,1} - h_{ex,s})$$

total-to-static efficiency at the rotor exit

$$\eta_{T-st} = (h_{0,1} - h_3)/(h_{0,1} - h_{3,s})$$

$D$  – wheel diameter

$h$  – enthalpy

$\dot{m}$  – mass flow rate

$M$  – Mach number

$P$  – power output of the turbine

$Q$  – volumetric flow rate

$R$  – Gas constant for the working fluid

$T$  – Temperature

$U$  – tip speed

$y^+$  – dimensionless wall distance

$\gamma$  – specific heat ratio

$\eta$  – isentropic efficiency

$\mu$  – dynamic viscosity

$\rho$  – density

$\omega$  – rotational speed

## Subscripts

0 – stagnation condition

1 – inlet to the nozzle

2 – inlet to the turbine

3 – exit from the turbine wheel

ex – discharge from the diffuser

s – isentropic state

n – nozzle

T-st – total-to-static

## References

- [1] Balje O E 1981 *Turbomachines* (John Wiley and Sons)
- [2] Kun L C and Sentz R N 1985 *Int. Conf. on Production and Purification of Coal Gas and Separation of Air* (Beijing) pp. 1-21
- [3] Ghosh P 2002 *Ph.D dissertation, IIT Kharagpur*
- [4] Moustapha H, Zelesky M F, Baines N C and Japikse D 2003 *Axial and Radial Turbines* (Concepts NREC)
- [5] Japikse D 2009 *SAE Technical Paper* 2009-01-0307
- [6] Verma R, Sam A A and Ghosh P 2015 *Phys. Procedia* **67** 373-78
- [7] Macchi E 1985 *Thermodynamics and Fluid Mechanics of Turbomachinery* **2** 805-28.
- [8] Ghosh S K 2010 *Int. J. Eng. Sci. Technol.* **2(1)** 175-91
- [9] Hasselgruber H 1958 Stromungsgerechte gestaltung der laufrader von radialcompressoren mit axialem laufradeintrict Konstruktion **10** (1) 22 (in German)
- [10] Galindo J, Fajardo P, Navarro R and Garcia-Cuevas L M 2013 *Appl. Energy* **103** 116-27
- [11] Simpson A T, Spence S W T and Watterson J K 2009 *ASME J. Turbomachinery* **131** 031010-1 - 15
- [12] Sam A A and Ghosh P 2014 Performance validation of a large scale helium turboexpander for cryogenic Applications through CFD 25<sup>th</sup> Nat. Symp. On Cryogenics (Hyderabad, India, 8-10 December 2014)
- [13] Menter F R 2009 *Int. J. Comput. Fluid Dynamics* **23** (4) 305-16
- [14] Galindo J, Hoyas S, Fajardo P and Navarro R 2013 *Eng. Appln. Of Comput. Fluid Mechanics* **7** (4) 441-60
- [15] Thomas R J, Dutta R, Ghosh P and Chowdhury K 2012 *Cryogenics* **52(7-9)** 375-81
- [16] Brost V Ruprecht, A and Maihofer M 2003 *Conf. on case studies in hyd. Systems (Belgrade)*
- [17] Baines N C 1998 *Inst. Mech. Eng. Conf. on Turbochargers* (UK: IMechE)